Convection heat transfer of colinear interacting droplets with surface mass transfer

H. Chiang and C. Kleinstreuer
Department of Mechanical and Aerospace Engineering, North Carolina State University, Raleigh, NC, USA

A validated computer simulation model has been developed for the analysis of colinear droplets in a heated gas stream. Using a finite-element method, the complete gas-phase transport equations have been solved describing quasi-steady laminar axisymmetric flow past closely spaced monodisperse constant-diameter droplets with blowing. The liquid-phase motion is represented by Hill's spherical vortex, coupling the gas-phase shear stress with the tangential surface velocity of the droplet. Of interest are the coupled nonlinear interaction effects on the fluid-flow patterns and temperature fields for different free-stream Reynolds numbers ($10 \leq Re \leq 200$), interdroplet distances ($1.5 \leq d_{ij} \leq 6.0$), liquid–gas viscosity ratios ($1 \leq \kappa \leq 100$), and Stefan or heat transfer numbers ($0 \leq BH \leq 5.0$). Surface mass transfer (blowing) and associated wake effects reduce both the total drag coefficient and the average Nusselt number for each interacting droplet when the Reynolds number increases. Large liquid–gas viscosity ratios, i.e., $\kappa > 20$, have hardly any effect on the drag coefficient and Nusselt number ratios. However, droplet spacings at $d_{ij} \leq 6$ and intermediate Reynolds numbers have a profound effect on all droplets, especially the second and third one, which experience significantly reduced drag and heat transfer at small interdroplet distances.

Keywords: closely spaced droplets; two-phase fluid mechanics; gas-phase heat transfer; Stefan number; viscosity ratio; finite element solution of Navier–Stokes equations

Introduction

Forced-convection heat transfer between Newtonian fluids and multiple evaporating droplets in a linear array is an important base-case system for analyzing the effects of droplet spacings, two-phase viscosity ratios, and evaporization rates on the drag/interaction coefficient, Nusselt number, and Sherwood number of each droplet relative to a solitary nonevaporating droplet. Engineering systems applications of interest include droplet sprays, dense fluid-particle fields, and two-phase flows.

Basic experimental and numerical studies of forced convection past a single vaporizing drop or a liquid sphere with surface mass transfer are well documented.[1–6] For example, Renksizbulut and Yuen[1] developed an empirical Nusselt number correlation $Nu = Nu(Re, BH, Pr)$ for a porous sphere, representing an evaporating droplet. Numerical studies[2,5,6] expanded on their experiments and included drag correlations and the effects of variable gas-phase properties. Conner and Elghobashi[3] provided a finite difference solution of laminar flow ($Re \leq 100$) past a liquid sphere with surface blowing, and demonstrated its measurable influence on flow separation, drag coefficient, wake length, and the average Sherwood number.

Detailed multiple-particle investigations are typically restricted to low Reynolds number flows past two solid spheres or vaporizing droplets in tandem. For example, Zaprynov and Toshev[7] solved numerically the complete transport equations for steady axisymmetric thermal flow around a pair of spheres at $Re \leq 40$. Raju and Sirignano[8] considered two vaporizing droplets, one following the other with an initial Reynolds number of $Re = 100$ for the leading droplet. In contrast, Kleinstreuer and Wang[9] used a relatively simple but sufficiently accurate, patched boundary-layer approach to analyze the dynamics of three interacting vaporizing fuel droplets on a one-dimensional (1-D) trajectory. Relevant experimental work is still limited to flow visualization and measurements of the drag coefficients for two-sphere systems[10,11] or for nonevaporating water drops on a two-dimensional (2-D) trajectory.[12] At least *three* particles have to be considered for the evaluation of realistic interaction effects. Such minimum particle configurations are computationally efficient and set the stage for more generalized analyses.

In this article we consider steady laminar axisymmetric flow ($10 \leq Re \leq 200$) past closely spaced monodisperse droplets ($1.5 \leq d_{ij} \leq 6.0$; $1 \leq \mu_l/\mu_g \leq 100$) of constant diameter and constant saturation temperature. Interfacial mass transfer in terms of the local blowing velocity $v_n(\theta)$ is being evaluated ($0 \leq BH \leq 5$). Thus, interacting vaporizing droplets are being analyzed under quasi-steady-state conditions as they may occur right after droplet heating to the saturation temperature, T_s. The present analysis is based on our previous works,[13,14] which dealt with convection heat transfer of multiple interacting solid spheres.

Analysis

Considering steady laminar axisymmetric flow of a heated Newtonian fluid past three colinear, monodisperse constant-diameter droplets of constant temperature and with shear-stress induced averaged internal circulation (Hill's spherical vortex), the governing dimensionless equations are (cf. Figure 1)

Gas phase:

$$\nabla \cdot \vec{v} = 0 \tag{1}$$

$$(\vec{v} \cdot \nabla)\vec{v} = -\nabla p + Re^{-1} \nabla^2 \vec{v} \tag{2}$$

$$(\vec{v} \cdot \nabla)T = Pe^{-1} \nabla^2 T \tag{3}$$

Address reprint requests to Professor Kleinstreuer at the Department of Mechanical and Aerospace Engineering, North Carolina State University, Raleigh, NC 27695-7910.

Received 31 May 1990; accepted 19 December 1990

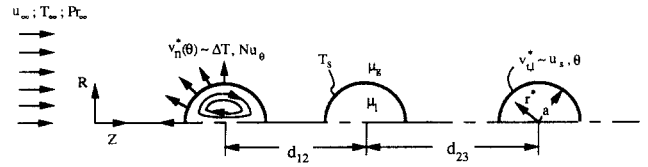

Figure 1 System schematics for three closely spaced droplets with surface mass transfer

The dimensionless variables are defined as

$$u=u^*/u_\infty,\quad v=v^*/u_\infty,\quad p=p^*/(\rho u_\infty^2),\quad T=(T^*-T_s)/(T_\infty-T_s),$$
$$r=r^*/d,\quad \mathrm{Re}=u_\infty d/\nu,\quad \text{and}\quad \mathrm{Pe}=u_\infty d/\alpha$$

Liquid phase:

$$v_r^*=u_s(1-r^{*2}/a^2)\cos\theta$$
$$v_\theta^*=-u_s(1-2r^{*2}/a^2)\sin\theta \tag{4}$$

where $u_s=v_\theta^*$ $(r^*=a,\ \theta=90°)$. Actually, the maximum slip velocity is obtained from a (frictional) force balance at the gas–liquid interface, viz.

$$\tfrac{1}{2}\pi a^2\rho_g u_\infty^2 C_F=8\pi a\mu_l u_s \tag{5a}$$

or

$$\frac{u_s}{u_\infty}=\frac{1}{32}\kappa^{-1}C_F\mathrm{Re} \tag{5b}$$

Thus, with Equation 5b, the tangential surface velocity $v_t^*=v_\theta^*$ $(r^*=a)$ can be computed. The underlying assumptions of droplet sphericity and negligible surface-tension effect imply that a conservative value for the Weber number of $\mathrm{We}\leq 4$ is recommended, as can be deduced from the papers by Sirignano[15] and others.[16–18] In addition, for the asymptotically steady-state case considered here, Hill's potential flow solution is a good approximation for the isothermal flow field inside the droplets. The normal velocity is obtained from an energy balance at the interface where it is assumed that the droplet is at the saturation temperature and heat transfer to the droplet's interior is negligible:

$$\Delta A_s h(T_\infty-T_s)=\Delta A_s\rho v_n^* L \tag{6a}$$

so that with $h=k_g\mathrm{Nu}/d$ we have

$$\frac{v_n^*}{u_\infty}=(\mathrm{Nu}\,\mathrm{BH})/\mathrm{Pe} \tag{6b}$$

While the heat transfer number or Stefan number $\mathrm{BH}=c_p(T_\infty-T_s)/L$ and the gas-phase Peclet number are input parameters, the local Nusselt number, $\mathrm{Nu}\sim\partial T/\partial r$ at $r=1/2$, has to be iteratively determined. As discussed earlier, although surface mass transfer (vapor injection) takes place, droplet shrinking is not being considered here.

The boundary conditions include

(i) at the inlet:

$$u=1,\ v=0,\ \text{and}\ T=1 \tag{7a}$$

(ii) along the centerline:

$$v=0,\ \partial u/\partial r=0,\ \text{and}\ \partial T/\partial r=0 \tag{7b}$$

(iii) at the fluid–solid interfaces:

$$\vec{v}=(v_t, v_n)\ \text{and}\ T=0 \tag{7c}$$

At all Reynolds numbers, the computational domain is large enough that all appropriate gradients are zero on the upper boundary and at the outlet of the region. This requires a mesh

Notation

A_s	Droplet surface area
a	Radius of droplet
BH	Heat transfer or Stefan number, $c_p(T_\infty-T_s)/L$
C	Drag coefficient
C_{Ds}	Total drag coefficient of single sphere without blowing
$C_D^{(k)}$	Total drag coefficient for droplet k
d	Droplet diameter
d_{ij}	Dimensionless interdroplet distances, $d_{ij}=d_{ij}^*(d)$
h	Heat transfer coefficient
L	Latent heat of vaporization
p	Pressure
Nu	Nusselt number, hd/k
Pr	Prandtl number, ν/α
Pe	Peclet number, Re Pr
R	Radial cylindrical coordinate
r	Radial spherical coordinate
Re	Reynolds number, $u_\infty d/\nu$
T	Temperature
$\vec{v}$	Velocity vector
v_n	Normal or local blowing velocity
v_t	Tangential components
u, v	Velocity components
u_s	Maximum slip velocity
u_∞	Characteristic or free-stream velocity
We	Weber number, $\mathrm{We}=\rho u_\infty^2 d/\sigma$
z	Axial coordinate

Greek symbols

α_k	Drag coefficient ratio for droplet k
β_k	Heat transfer coefficient ratio for droplet k
κ	Liquid–gas viscosity ratio, μ_l/μ_g
ν	Kinematic viscosity
ρ	Density
θ	Spherical coordinate
θ_{sep}	Separation angle measured from forward stagnation point
σ	Surface tension

Subscripts

b	Surface blowing
d	Based on diameter
D	Total drag
F	Friction
g	Gas phase
i	Index for particle spacing $(i=1, 2)$
j	Index for particle spacing $(j=i+1)$
k	Index for particle identification $(k=1, 2, 3)$
l	Liquid phase
P	Pressure
s	Single droplet, saturation, surface
sep	Flow separation
T	Thrust
∞	At infinity

Superscripts

*	Dimensional quantities
(k)	Index for droplet

that increases in lateral extent with decreasing Reynolds numbers and in length with larger Reynolds numbers.

Numerical solution method

The governing equations (Equations 1–3), subject to conditions 4a, 4b, and 7a–7c, are solved using a widely accepted finite-element software package.[19] Actually, the penalty function approach is used where the continuity requirement is weakened by replacing Equation 1 with $\nabla\cdot\mathbf{v}=\varepsilon p$, where the penalty parameter ε is very small, that is, $\varepsilon=\mathcal{O}(10^{-6})$. The elements chosen are isoparametric quadrilaterals with nine nodes. Bi-quadratic shape functions are selected for approximating velocity and temperature profiles, whereas the pressure is given by discontinuous linear shape functions.[20] The solution is started from a low Reynolds number, say, $\mathrm{Re}=10$, and then with the converged steady-state solution, the free-stream Reynolds number and surface blowing are gradually increased. Specifically, first a normal velocity, e.g., $v_n(\theta)=0$, and a related tangential velocity (cf. Equation 4) are specified. Then Equations 1–3 are solved subject to the boundary conditions 7a–7c. With the given gas flow and temperature fields, a new set of interfacial velocity components can be obtained from Equations 5b, 4, and 6b. Computations proceed iteratively until variations of these surface velocities are less than 10^{-4}. A quasi-Newton algorithm is used for solving the nonlinear equations with a reformation of the Jacobian matrix every five steps. In order to facilitate convergence, a slower but more robust successive substitution method is applied for the first three steps to bring the solution within the radius of convergence of the quasi-Newton method. Subsequently, the faster converging quasi-Newton scheme is invoked. A complete run, i.e., the velocity, pressure, and temperature fields for, say, $\mathrm{Re}=100$ and $\mathrm{BH}=2.0$, takes about 8 minutes on a CRAY Y-MP.

A mesh of variable density is required for cost-effective computer runs. Typically, a total of 6000 nodal points, where $\Delta\theta=3.2°$ on the droplet surface, are needed. Very small elements are placed at the interface and large elements near the domain boundaries. A smooth transition from fine to coarse mesh regions has been achieved. The overall mesh size has been obtained in accordance with the boundary conditions by trial and error. Specifically, the location of the upper domain boundary is about $16a$ when $\mathrm{Re}\leq 20$ and $12a$ for $\mathrm{Re}\geq 100$, where a is the droplet radius. Independence of the simulation results from the mesh density has been successfully tested based on repeat calculations with finer meshes.

With the given postprocessing capabilities, wall heat flux calculations as well as plots of velocity vector fields, pressure surfaces, isotherms, and temperature surfaces can be conveniently executed.

Results and discussions

The numerical code has been verified with published data sets for solitary spheres (Table 1), single vaporizing droplets (Table 2), and two-sphere systems.[14] The empirical correlations for the single-sphere separation angle, $\theta_{sep,s}=\theta(\tau_s=0)$, the total drag coefficient, $C_{Ds}=8F_D/(d^2\pi\rho u^2)$, and the average Nusselt number, $\overline{\mathrm{Nu}}_s=\bar{h}d/k$, are given in Clift et al.[21]

$$\theta_{sep,s}=180-42.5\left(\ln\frac{\mathrm{Re}}{20}\right)^{0.483} \quad \text{for} \quad 20<\mathrm{Re}<400 \tag{8}$$

$$C_{Ds}=\frac{24}{\mathrm{Re}}(1+0.1935\mathrm{Re}^{0.6305}) \quad \text{for} \quad 20<\mathrm{Re}<260 \tag{9}$$

$$\frac{\overline{\mathrm{Nu}}_s-1}{\mathrm{Pr}^{1/3}}=[1+(\mathrm{RePr})^{-1}]\mathrm{Re}^{0.41} \quad \text{for} \quad \begin{cases}1<\mathrm{Re}<400\\ 0.25<\mathrm{Pr}<100\end{cases} \tag{10}$$

For a single vaporizing droplet model, Renksizbulut and Yuen[1] developed an empirical Nusselt number correlation

$$\overline{\mathrm{Nu}}(1+\mathrm{BH})^{0.7}=2+0.57\mathrm{Re}^{1/2}\mathrm{Pr}^{1/3} \tag{11}$$

Table 1 Comparison of characteristic parameters for thermal flow past a sphere

	Separation angle, $\theta_{sep,s}$		Drag coefficient, C_{Ds}		Nusselt no., $\overline{\mathrm{Nu}}_s$ (Pr = 1.0)		Blowing effect $C_{Ds,b}/C_{Ds}$	
Re	Model	Eq. 8	Model	Eq. 9	Model	Eq. 10	Model	Hamielec et al.[22]
10	—	—	4.37	4.38	3.59	3.65	—	—
20	—	—	2.75	2.73	4.32	4.37	—	—
40	144.4	144.0	1.80	1.79	5.53	5.57	0.86	0.87
50	139.5	139.3	1.60	1.57	6.01	6.00	—	—
100	125.1	126.5	1.09	1.08	7.70	7.63	0.84	0.85
200	116.5	116.4	0.77	0.77	9.79	9.80	—	—

Table 2 Comparison of total drag coefficient and averaged Nusselt number for a vaporizing droplet model

		Drag coefficient, C_D		Nusselt number, $\overline{\mathrm{Nu}}$	
$\mathrm{Re}=u_\infty d/\nu$	$\mathrm{BH}=c_p\Delta T/L$	Present work	Renksizbulut and Yuen[2]	Present work	Equation 11
40	0.0	1.802	1.826	5.000	5.200
	0.51	1.611	1.683	3.840	3.916
	2.0	1.432	—	2.455	2.410
	3.46	1.378	—	1.862	1.826
100	0.213	1.044	1.071	6.164	6.168
	0.462	1.000	1.032	5.475	5.413
	0.783	0.964	0.992	4.787	4.711
	1.75	0.908	—	3.547	3.478
	5.0	0.862	—	2.016	2.014

that can be applied in the ranges $25 \leq Re \leq 2000$ and $0.07 \leq BH \leq 2.79$. Their model[1] had a very large viscosity ratio (gas-stream/blowing sphere model), and therefore internal circulation could not be accounted for. The fluid properties were evaluated at a film temperature taken as the average of the free-stream temperature and the "droplet" surface temperature. The agreement (cf. Table 2) is within 3%, although concentration-driven mass transfer has been neglected.

Fluid-flow patterns

The fluid mechanics in terms of velocity vector plot and pressure surface plot for gas flow past three closely-spaced non-evaporating droplets is shown in Figures 2a and 2b. For these representative conditions ($Re = 100$, $\kappa = 10$, and $d_{12} = d_{23} = 1.5$), the tangential droplet surface velocity can be substantial (cf.

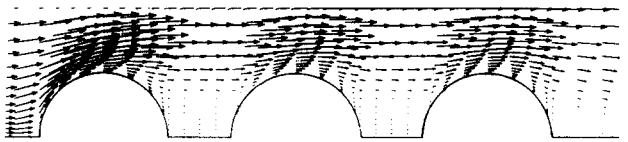

Figure 2(a) Velocity vector plot for interacting nonevaporating droplets ($Re = 100$, $\kappa = 10$, and $d_{12} = d_{23} = 1.5$)

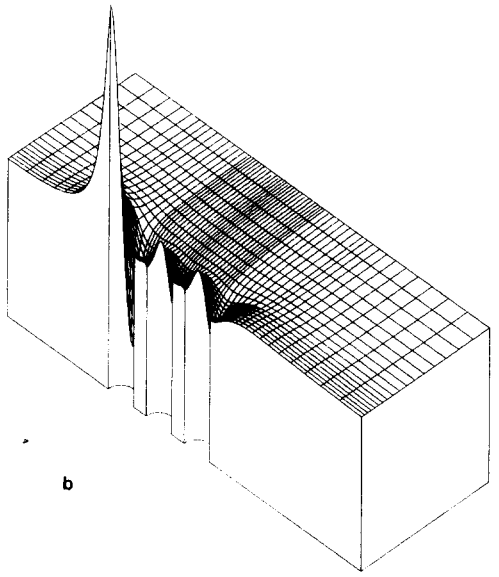

Figure 2(b) Pressure surface plot for interacting nonevaporating droplets ($Re = 100$, $\kappa = 10$, and $d_{12} = d_{23} = 1.5$)

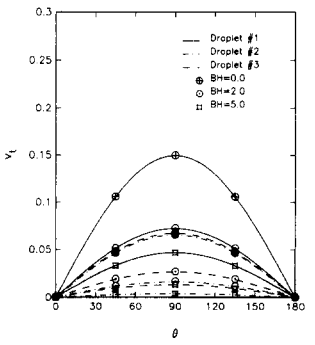

Figure 3 Effect of heat transfer number $BH \sim \Delta T$ on local tangential velocity at gas–liquid interface ($Re = 100$, $\kappa = 10$, and $d_{12} = d_{23} = 1.5$)

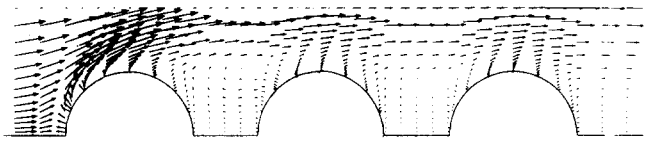

Figure 4 Velocity vector plot for interacting droplets with blowing ($Re = 100$, $\kappa = 10$, and $d_{12} = d_{23} = 1.5$, and $BH = 5.0$)

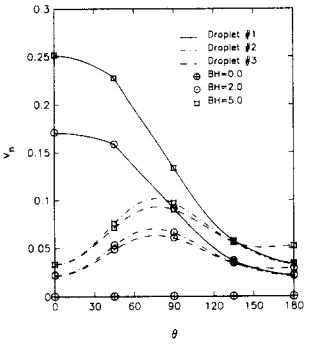

Figure 5 Effect of heat transfer number $BH = 0$, 2, 5 on local blowing velocity or local Nusselt number of each droplet ($Re = 100$, $\kappa = 10$, and $d_{12} = d_{23} = 1.5$)

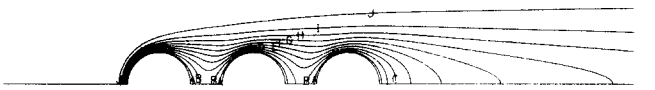

Figure 6 Gas-phase isotherms of interacting nonevaporating droplets ($Re = 100$, $\kappa = 10$, and $d_{12} = d_{23} = 1.5$)

Figure 3: $0 \leq v_t^*/u_\infty \leq 0.15$), delaying flow separation and contributing to small, slowly recirculating fluid zones between the closely spaced droplets (cf. Figure 2a). The pressure, acting in correspondence to the velocity field, peaks at the forward stagnation point of the first droplet, reaches a maximum negative value at $\theta \approx 90°$, and then recovers in a relatively low-pressure wake region with two mild pressure peaks at the reattachment points of droplets 2 and 3 (cf. Figure 2b). The effect of the heat transfer number, $BH \sim \Delta T \sim v_n(\theta)$, is shown in Figures 4 and 5. The velocity field (Figure 4) is now strongly influenced by vapor injection (cf. Figure 5: $0.03 \leq v_n^*/u_\infty \leq 0.25$), which decelerates the bulk gas flow, creates radially extended recirculation regions between the droplets, and increases the boundary-layer thicknesses substantially. As a result, the velocity field (and the temperature field) are rather similar for droplets 2 and 3 as well as fairly symmetric in $0 \leq \theta \leq 180$.

Temperature contour plots

The gas-phase isotherms and temperature surface plots for different spacings and heat transfer numbers are shown in Figures 6 to 8b for $Re = 100$ and $\kappa = 10$. Fluid injection (e.g., $BH = 5$) thickens the thermal boundary layer, resulting in reduced temperature gradients, which imply lower Nusselt numbers (cf. Figure 6 *versus* Figure 7a). After the first droplet, the temperature field in the direct vicinity of droplets 2 and 3 is drastically reduced and rather similar (cf. Figures 6 to 7b). At larger intersphere distances ($d_{ij} \geq 6.0$), the temperature field after the first droplet may recover leading to somewhat symmetric profiles for droplets 2 and 3 (cf. Figures 8a and 8b).

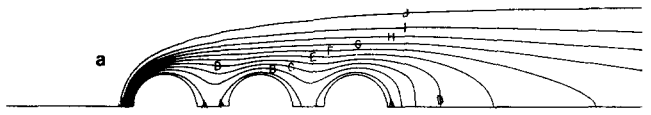

Figure 7(a) Gas-phase isotherms of interacting droplets with surface mass transfer (Re = 100, $\kappa = 10$, $d_{12} = d_{23} = 1.5$, and BH = 5)

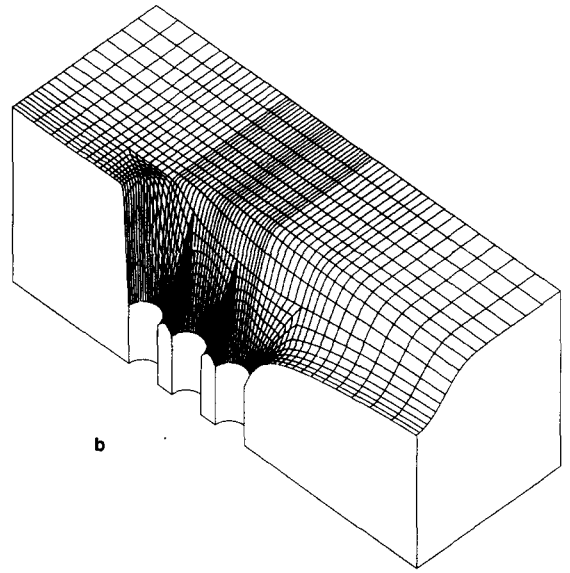

Figure 7(b) Temperature surface plot for interacting droplets with surface mass transfer (Re = 100, $\kappa = 10$, $d_{12} = d_{23} = 1.5$, and BH = 5)

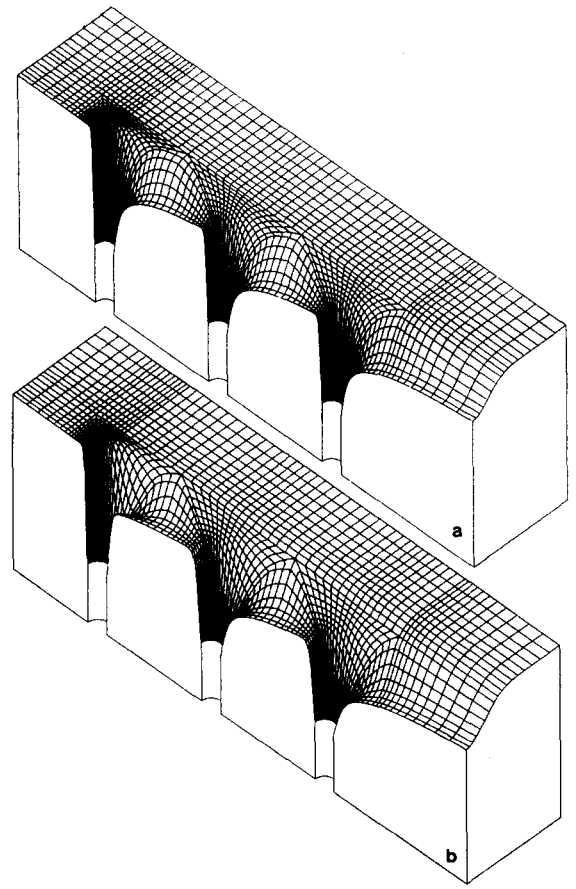

Figure 8(a) Temperature surface plots for nonevaporating droplets at larger spacings (Re = 100, $\kappa = 10$, and $d_{12} = d_{23} = 6.0$)

Figure 8(b) Temperature surface for widely spaced droplets with surface mass transfer (Re = 100, $\kappa = 10$, $d_{12} = d_{23} = 6.0$, and BH = 5)

Integral parameters: ratios of total drag coefficients and averaged Nusselt numbers

The drag coefficient ratio is defined as

$$\alpha_k \equiv C_D^{(k)}/C_{Ds} \tag{12}$$

where $C_D^{(k)}$ is the drag/interaction coefficient of droplet k and C_{Ds} is the single nonevaporating droplet drag coefficient. As $d_{ij} \to \infty$, $\kappa \gg 1$ or $v_t = 0$, and BH $\equiv 0$, $\alpha_k \to 1$. The total drag consists of friction, pressure, and thrust drag, i.e.,

$$C_F = -4 \int_0^{\pi} \tau_{r\theta}|_{r=1/2} \sin^2 \theta \, d\theta \tag{13a}$$

$$C_P = 2 \int_0^{\pi} p|_{r=1/2} \sin 2\theta \, d\theta \tag{13b}$$

and

$$C_T = 4 \int_0^{\pi} (v_n^2 \cos \theta - v_n v_t \sin \theta) \sin \theta \, d\theta \tag{13c}$$

Figures 9a to 10b show α_k at Re = 100 for different spacings as a function of viscosity ratio $\kappa = \mu_l/\mu_g$ and Stefan number BH $\sim \Delta T$. Figure 9a when compared to Figure 9b indicates the

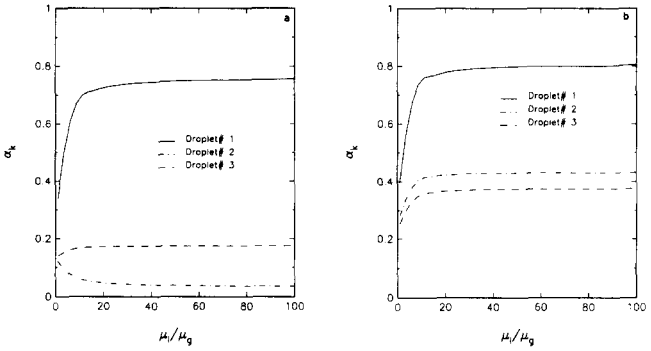

Figure 9(a) Effect of viscosity ratio on drag coefficient ratio for each closely spaced droplet (Re = 100, $d_{12} = d_{23} = 1.5$, and BH = 2)

Figure 9(b) Effect of viscosity ratio on drag coefficient ratio for each widely spaced droplet (Re = 100, $d_{12} = d_{23} = 6.0$, and BH = 2)

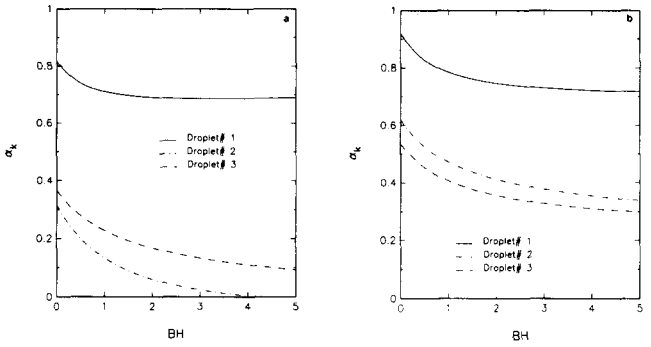

Figure 10(a) Effect of heat transfer number on drag coefficient ratio for each closely spaced droplet (Re = 100, $d_{12} = d_{23} = 1.5$, and $\kappa = 10$)

Figure 10(b) Effect of heat transfer number on drag coefficient ratio for each widely spaced droplet (Re = 100, $d_{12} = d_{23} = 6.0$, and $\kappa = 10$)

strong nonlinear interaction effect of neighboring droplets. At relatively low viscosity ratios, $\kappa \lesssim 10$, the tangential interface or "slip" velocity is rather large, causing lower (friction) drag, especially for the first droplet. However, at narrow interdroplet spacings (cf. Figure 9a), the second droplet experiences a negative C_p (cf. Figure 2b), resulting in an α_2 smaller than α_1 and α_3. At larger spacings (cf. Figure 9b), pressure recovery after the first (and second) droplet yields typical $\alpha_k(\kappa)$-curves at higher levels than for small spacings. For $\kappa \geq 20$, the maximum slip velocity falls below 10% of the free-stream velocity (at Re = 100) and the drag coefficient ratio becomes independent of the viscosity ratio. The effects of the heat transfer number and interdroplet spacing on the total drag of each interacting droplet is shown in Figures 10a and 10b for a typical air-stream fuel droplet combination. Increasing surface mass transfer (e.g., BH > 3) generates more uniform conditions, i.e., gradients and fluxes, near the droplets, resulting in mildly varying integral parameters. At larger spacings, here $d_{ij} = 6.0$, α_k of the leading droplet reaches almost unity for BH = 0 (cf. Figure 10b). The remaining difference, i.e., $1 - \alpha_1$, is due to interfacial slip and finite spacing.

The Nusselt number ratio is defined as

$$\beta_k \equiv \overline{\mathrm{Nu}^{(k)}} / \overline{\mathrm{Nu}_s} \tag{14}$$

i.e., the averaged Nusselt number of the interacting droplet k *versus* the Nusselt number of a solitary nonevaporating droplet. Here,

$$\overline{\mathrm{Nu}^{(k)}} = \frac{1}{2} \int_0^{\pi} \mathrm{Nu} \sin\theta \, d\theta \tag{15a}$$

where the local Nusselt number is

$$\mathrm{Nu} = \frac{hd}{k} = -\left.\frac{\partial T}{\partial r}\right|_{r=1/2} \tag{15b}$$

The local Nusselt number can be directly obtained from Equation 6b, viz.,

$$\mathrm{Nu}^{(k)}(\theta) = \frac{\mathrm{Pe}}{\mathrm{BH}} v_n^{(k)}(\theta), \qquad \mathrm{BH} > 0 \tag{16}$$

Thus, Figure 5 depicts the local Nusselt number behavior of each closely spaced droplet for BH = 2.0 and 5.0.

As indicated in Figures 11a and 11b, at about zero surface mass transfer, the first droplet exhibits a higher average Nusselt number than the associated single droplet, i.e, $\beta_1 > 1.0$, because of the slip velocity that reduces the wake and hence increases the surface area of more intense heat transfer. The β_k(BH)-curves for the closely-spaced droplets 2 and 3 (cf. Figure 11a) are significantly reduced but similar because of the unique fluid-flow field created by the first droplet. At larger spacings, the thermal flow recovers and β_k(BH)-curve for $k = 2, 3$ move closer to β_1(BH) as shown in Figure 11b.

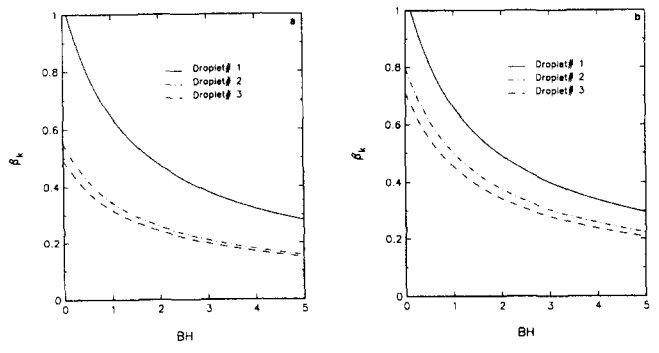

Figure 11(a) Effect of heat transfer number on Nusselt number ratio for each closely spaced droplet (Re = 100, $\kappa = 10$, and $d_{12} = d_{23} = 1.5$)

Figure 11(b) Effect of heat transfer number on Nusselt number ratio for each widely spaced droplet (Re = 100, $\kappa = 10$, and $d_{12} = d_{23} = 6.0$)

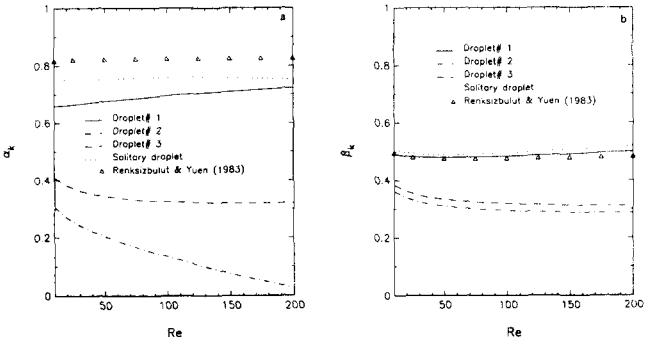

Figure 12(a) Effect of Reynolds number on drag coefficient ratio for each droplet (BH = 2, $\kappa = 10$, $d_{12} = 2$, and $d_{23} = 4$)

Figure 12(b) Effect of Reynolds number on Nusselt number ratio for each droplet (BH = 2, $\kappa = 10$, $d_{12} = 2$, and $d_{23} = 4$)

The influence of varying free-stream Reynolds number on the drag coefficient ratio α_k and on the heat transfer coefficient ratio β_k is shown in Figures 12a and 12b for BH = 2, $\kappa = 10$, $d_{12} = 2$, and $d_{23} = 4$. For comparison, α and β of a solitary vaporizing droplet as well as measured data points for the "blowing sphere" of Renksizbulut and Yuen[1] are included. The dotted single-droplet curves indicate (the) interaction effects of multiple droplets on the momentum transfer (Figure 12a) and heat transfer (Figure 12b). The triangles[1] depict, relative to the solitary droplet, the effect of internal circulation and hence "surface slip" (or viscosity ratio) on α and β. Clearly, a surface slip velocity reduces both friction and pressure drag (cf. Figure 12a) while the convective heat transfer is slightly enhanced (cf. Figure 12b).

Focusing on Figure 12a, it is apparent that the drag coefficient ratio of the single droplet is hardly affected by the gas-stream velocity for BH = 2, while α_1(Re) increases gradually. In contrast, α_2 is much lower than α_1 (and α_3) and decreases significantly with increasing Reynolds number due to "similar" fro/aft recirculation regions causing smaller form or pressure drag (cf. Figure 4); because of the higher pressure drag, $\alpha_3 > \alpha_2$.

Figure 12b shows β_1(Re) mildly increasing and, at a lower magnitude, $\beta_{2,3}$(Re) decreasing, where $\beta_2 < \beta_3$. Surface blowing, i.e., fluid injection at the droplet temperature, thickens the thermal boundary layer and mitigates the Reynolds number effect. Multiparameter correlations for α_k and β_k considering three interacting spheres with blowing are given elsewhere.[23]

Conclusions

The steady-state Navier–Stokes and heat transfer equations describing laminar, axisymmetric, heated gas flow past closely spaced colinear droplets with internal circulation and surface mass transfer have been solved using a finite-element method. Of interest are the effects of free-stream Reynolds number, interdroplet spacing, gas–liquid viscosity ratio, and Stefan number on the quasi-steady fluid-flow field (including individual drag coefficients) and temperature field (including individual Nusselt numbers). The results of the validated computer simulation model can be summarized as follows.

- Higher Reynolds numbers decrease the penetration depth or boundary-layer thickness and increase the surface tangential

velocity because of larger interfacial shear stress. The total drag coefficient of the *first* droplet may increase slightly with increasing Reynolds number for strongly interacting, i.e., very closely spaced droplets. Surface blowing and associated wake effects reduce both the total drag coefficient and the average Nusselt number for each interacting downstream droplet when the Reynolds number increases.

- Droplet spacings have a profound effect on the fluid mechanics and heat transfer of multiple droplets. At large spacings, $d_{ij} > 6$, and intermediate Reynolds numbers, $\mathrm{Re} < 200$, the pressure and velocity field may recover after each droplet, resulting in integral parameters, e.g., α_k and β_k, close to ones for solitary droplets with equivalent heat transfer numbers. However, at small spacings the drag is lower for each particle. Especially the drag of the droplets behind the leading droplet may be significantly reduced, leading to imminent particle collision. Heat transfer is also diminished at small spacings, changing the evaporation rate and shifting the points of maximum blowing velocity downstream.
- Changes in the liquid–gas viscosity ratio from, say, $\kappa = 10$ for water drops in an air system to $\kappa = 1$ representing gas bubbles in a gas stream, result in very large surface tangential velocities, which in turn reduce the drag coefficients measurably. However, for systems with $\kappa > 20$, α_k and β_k are unaffected.
- An increase in heat transfer or Stefan number, $\mathrm{BH} \sim \Delta T$, increases surface mass transfer, which reduces the tangential velocity at the interface because of reduced shear stress. As a result, the heat transfer ratio number β_k is lowered. In general, surface blowing, which is strongest at the forward stagnation or flow reattachment points, thickens the boundary layers and generates milder velocity and temperature gradients. Consequently, the (local) Nusselt number is reduced, and hence the local blowing velocity is a dynamic balance of the prescribed temperature difference, $\Delta T = T_\infty - T_s$, and the resulting convection heat transfer at the interface, $\mathrm{Nu} \sim \partial T / \partial r$.

Future work will concentrate on the transient dynamics of multiple interacting vaporizing droplets. Ultimately, the restrictions of laminar axisymmetric flow have to be lifted for a more realistic simulation of *dense* fluid-particle flow fields.

Acknowledgments

This work has been supported in part by the Department of Energy, Office of Basic Energy Science, grant No. DE-FG05-87ER13728. The support of the North Carolina Supercomputing Center (NCSC) under an Advanced Computing Resources Grant is greatly appreciated.

References

1 Renksizbulut, M. and Yuen, M. C. Experimental study of droplet evaporation in a high-temperature air stream. *J. Heat Transfer*, 1983, **105**, 384–388

2 Renksizbulut, M. and Yuen, M. C. Numerical study of droplet evaporation in a high-temperature stream. *J. Heat Transfer*, 1983, **105**, 389–397

3 Conner, J. M. and Elghobashi, S. E. Numerical solution of laminar flow past a sphere with surface mass transfer. *Num. Heat Transfer*, 1987, **12**, 57–82

4 Ryskin, G. Heat or mass transfer from a moving drop—some approximation relations for the Nusselt number. *Int. Comm. Heat Mass Transfer*, 1987, **14**, 741–749

5 Haywood, R. J., Nafziger, R., and Renksizbulut, M. A detail examination of gas and liquid phase transient processes in convective droplet evaporation. *J. Heat Transfer*, 1989, **111**, 495–502

6 Chiang, C. H., Raju, M. S., and Sirignano, W. A. Numerical analysis of convecting vaporizing fuel droplet with variable properties. AIAA Paper 89-0834, 1989

7 Zaprynov, Z. D. and Toshev, E. T. Hydrodynamics and heat transfer around two separated spherical particles. *Proc. 8th Int. Conf. on Heat Transfer*, San Francisco, 1986, **5**, 2549–2553

8 Raju, M. S. and Sirignano, W. A. Interaction between two vaporizing droplets in an intermediate Reynolds number flow. *Phys. Fluids A*, 1990, **2**(10), 1780–1796

9 Kleinstreuer, C. and Wang, T-Y. Approximate analysis of interacting vaporizing fuel droplets. *Int. J. Multiphase Flow*, 1990, **16**(2), 295–304

10 Rowe, P. N. and Henwood, G. A. Drag forces in a hydraulic model of a fluidized bed—Part I. *Trans. Inst. Chem. Engineers*, 1961, **39**, 43–56

11 Tsuji, Y., Morikawa, Y., and Terashima, K. Fluid-dynamic interaction between two spheres. *Int. J. Multiphase Flow*, 1982, **8**, 71–82

12 Mulholland, J. A., Srivastava, R. K., and Wendt, J. O. L. Influence of droplet spacing on drag coefficient in nonevaporating monodisperse streams. *AIAA J.*, 1988, **26**(10), 1231–1237

13 Ramachandran, R. S., Kleinstreuer, C., and Wang, T-Y. Forced convection heat transfer of interacting spheres. *Num. Heat Transfer*, 1989, Part A, **15**, 471–487

14 Ramachandran, R. S., Wang, T-Y., Kleinstreuer, C., and Chiang, H. Fluid flow characteristics of three closely-spaced monodisperse spheres or nonevaporating drops at low to moderate Reynolds numbers. *AIAA J.*, 1991, **29**(1), 43–51

15 Sirignano, W. A. Fuel droplet vaporization and spray combustion theory. *Prog. Energy Combust. Sci.*, 1983, **9**, 291–322

16 Pilch, M. and Erdman, C. A. Use of breakup time data and velocity history data to predict the maximum size of stable fragments for acceleration-induced breakup of a liquid drop. *Int. J. Multiphase Flow*, 1987, **13**, 741–757

17 Dandy, D. S. and Leal, L. G. Buoyancy-driven motion of a deformable drop through a quiescent liquid at intermediate Reynolds numbers. *J. Fluid Mech.*, 1989, **208**, 161–192

18 Hass, F. C. Stability of droplets suddenly exposed to a high velocity gas stream. *AIChE J.*, 1964, **10**, 920–924

19 Engelman, M. S. *FIDAP 5.0 Manuals, Volumes 1 to 3*, FDI, Evanston, IL, 1990

20 Cuvelier, C., Segal, A., and Van Steenhoven, A. A. *Finite Element Methods and Navier–Stokes Equations*, D. Reidel Publishing Company, Dordrecht, Holland, 1986

21 Clift, R., Grace, J. R., and Weber, M. E. *Bubbles, Drops and Particles*, Academic Press, New York, 1978

22 Hamielec, A. E., Hoffman, T. W., and Ross, L. L. Numerical solution of the Navier–Stokes equation for flow past spheres. *AIChE J.*, 1967, **13**(2), 212–219

23 Kleinstreuer, C. and Chiang, H. Convection heat transfer of closely-spaced spheres with surface blowing. Wärme & Stoffübertragung